CHAPTER II

LITERATURE REVIEW

Before the details of the present study are given , a brief review of the previous works on experimental study and numerical approach for the flow past an obstacle with infinite extent and also for the flow separation of internal flow are first made.

2.1 FLOW PAST AN OBSTACLE WITH INFINITE EXTENT

The general form of the flow past an obstacle especially the flat plate in fluid stream of infinite extent has been known for many years past. Various theories for calculating or explanation the resistance of the plate have also been advanced rom time to time.

Rayleigh (1876) presented the theory of *discontinuous* motion to predict a drag coefficient for an inclined flat plate in an infinite flow field at an angle α to the main stream

$$C_D = \frac{2\pi \sin \alpha}{(4 + \pi \sin \alpha)} \qquad (2.1)$$

This classical free-streamline theory does describe some of the general features of the mean flow such as the free-vortex layer and the constant pressure behind the plate.

Karmann (1911) proposed a formula for the resistance of a flat plate moving normal to the stream , in terms of the dimensions of the vortex system

behind the plate (see figure 2.1). This formula , given in the symbols of the paper , is

$$C_D = 0.281\,(a/b)\left[\,2.83\left(1 - \frac{V_3}{V_0}\right) - 1.12\left(1 - \frac{V_3}{V_0}\right)^2\,\right] \qquad (2.2)$$

If the second term be neglected the formula reduces to the approximate form

$$C_D = 0.795\,(a/b)\left(1 - \frac{V_3}{V_0}\right) \qquad (2.3)$$

which be shown the drag is then proportional to the strength of the individual vortices.

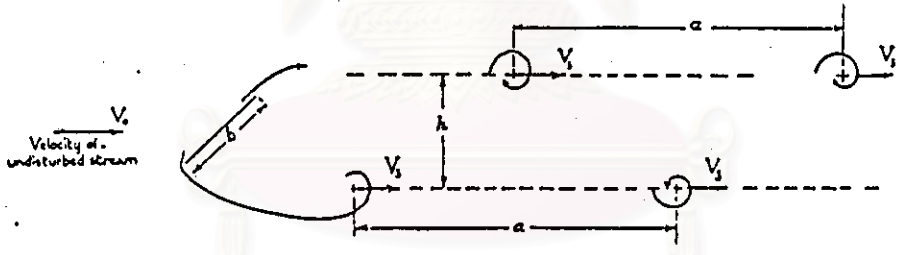

Figure 2.1 Vortex street.

where V_0 is velocity of the undisturbed air relative to the plate.

V_3 is downstream velocity of the individual vortices (V_3 = f.a).

f is frequency per second with which the individual vortices leave each edge of the plate.

a is longitudinal spacing between two consecutive vortices in the same row.

b is breadth of plate.

Fage and Johansen (1927) investigated the experiments of air flow behind an inclined flat plate of infinite span. A comparison was made between the measured values of drag and those obtained from two Karmann's formulae , when the wind tunnel values of (a / b) and (V_s / V_0) are substitued , is given in table 2.1.

α°	Wind-tunnel.		k_D.	k_D.		Col. B / Col. A	Col. C / Col. A
	(a/b)	(V_s/V_0)	k_D. (A)	Kármán's formula. (B)	Kármán's approx. formula. (C)		
90	5·25	0·765	1·065	0·895	0·980	0·84	0·92
70	4·85	0·755	0·975	0·855	0·945	0·88	0·97
60	4·44	0·760	0·850	0·770	0·850	0·91	1·00
50	4·08	0·790	0·690	0·625	0·680	0·91	0·99
40	3·55	0·815	0·505	0·485	0·520	0·96	1·03
30	2·76	0·840	0·325	0·335	0·350	1·03	1·08

Table 2.1 Comparison of drag coefficient.
(k_D is equivalent to C_D)

With summary , the vortices generated at each edge pass downstream with a frequency which increases as the inclination of the plate decreases. The

frequency is proportional to the wind speed , at a constant inclination. The longitudinal spacing of the vortices decreases as the inclination of the plate decreases.

Abernathy (1962) extended the modified free-streamline theory to include an inclined flat plate in an infinite flow field. At an arbitrary angle of attack , and with an experimental investigation of the behavior of the flow field in the vicinity of an inclined plate in a constricting flow channel. There is excellent agreement between theory and experiment regarding the pressure distribution for the case of relatively little lateral restriction of flow when K = 14.0 ; (K is dimensionless constriction ratio between height of tunnel test-section and plate chord) ; the agreement is only fair when K = 5.27 as shown in figure 2.2.

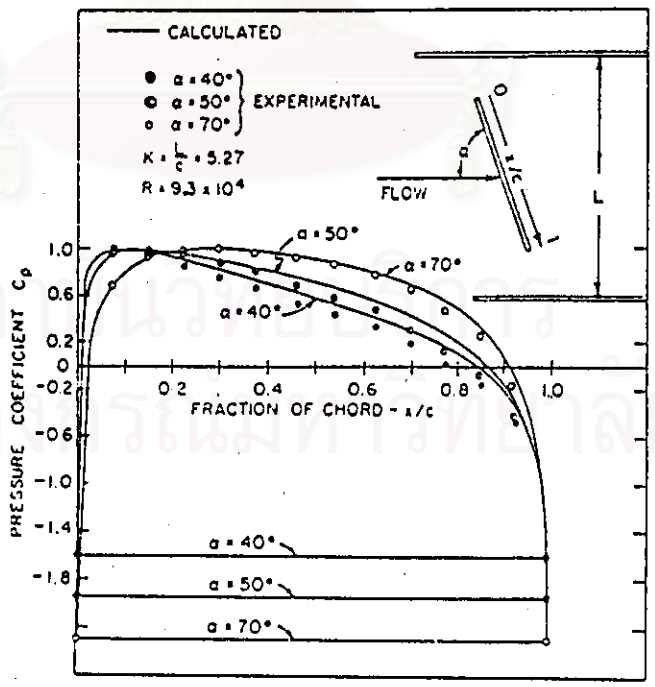

Figure 2.2 Calculated and experimental pressure coefficients on inclined sharp-edged plates for K = 5.27.

where C_P is *local pressure coefficient* and defined as

$$C_P = \frac{P - P_0}{(1/2)\rho V_0^2} \qquad (2.4)$$

where P is local static pressure.

and P_0 is free-stream static pressure.

Furthermore , the location of the free streamlines also was calculated and compared with the experimental results as shown in figure 2.3 for the location of the outer and inner boundaries of the free-vortex layers emanating from the leading and trailing edges of the flat plates of different chord length at varying incidences.

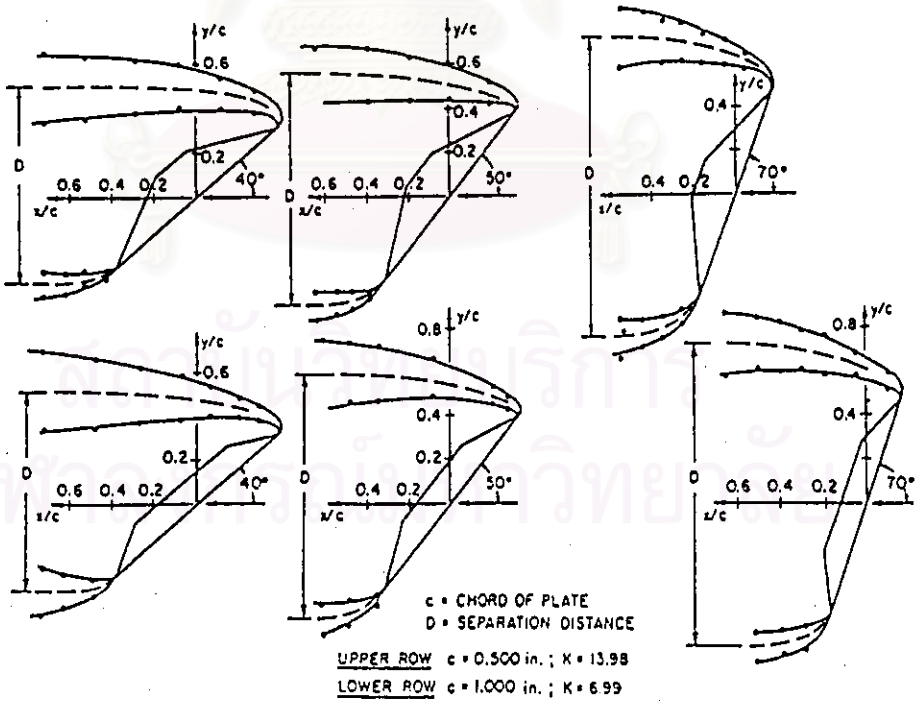

Figure 2.3 Free-vortex layers from inclined sharp-edged plates with lateral flow constriction : K = 13.98 and 6.99.

The solid circles are the points of either maximum or minimum mean velocity.The broken line is simply the locus of points midway between the outer and inner boundaries of the free-vortex layers. The length D is simply referred to as separation distance , measured perpendicularly to the free-stream direction , between the median lines in both free-vortex layers where the two median lines have become parallel. It is apparent that the separation distance is essentially independent of the constriction ratio from at least 14 to 5.27 , and is approximately equal to $\sqrt{2}.c.\sin\alpha$.

Chen and Cheng (1987) studied on finite analytic numerical solutions of incompressible flow past inclined axisymmetric bodies. The Navier-Stokes equations are solved by *FANS-3DEF* program which is based on the finite analytic method on the body-fitted coordinate system with modified SIMPLER algorithm. Some example of flow prediction is presented as shown in figure 2.4 gives the solution of a 10 degree angle of attack for Re = 2.48×10^6. One finds that a very small separation exists at the leading edge , also a strong separation around the trailing edge on the upper side of the plate.

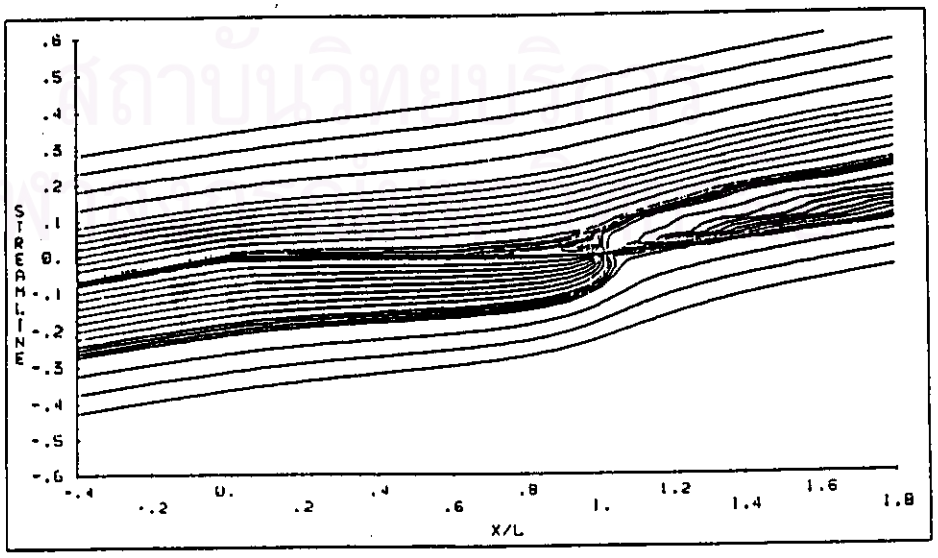

Figure 2.4 Streamline distribution at 10 degree angle of attack.

Ramamurthy , Balachandar and Vo (1989) undertook to develop a semi-empirical relation for the drag force experienced by constrained bluff bodies with separating edges. The governing equations are derived on the basis of a simple momentum balance with following assumptions.

1) For a given blockage , the pressure P_s at the separating point is independent of Reynolds number Re = Ub/ν. Here b is the width of the bluff body and ν is the fluid kinematic viscosity.

2) The back pressure P_b immediately behind the body is essentially the same as the separation pressure P_s.

3) The boundary friction is negligible along the control surfaces.

A control volume is chosen , denoted by the line joining points *E* , *F* , *G* , *H* , *I* , *J* , *K* and *L* as shown in figure 2.5

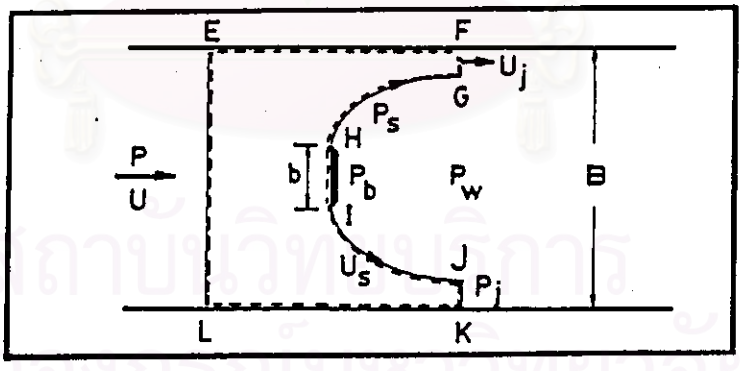

Figure 2.5 Constricted flow past flat plate.

where B is test-section width.

b is width of bluff body.

P is free-stream pressure.

P_w is wake pressure.

P_j is contracting jet pressure.

U is mean velocity upstream of the body.

U_j is mean velocity at the vena contracta.

U_s is velocity at separation.

After deriving and simplifying , the formula to calculate the drag coefficient was obtained

$$C_D = \frac{B}{b}\left[2.0 - C_{P_s} - \frac{1}{K_j}\left(1.0 - C_{P_s} - K_j^2\right) - 2\beta K_j \right] \quad (2.5)$$

where β is defined to be momentum coefficient as

$$\beta = 1 + \varepsilon^2 \quad (2.6)$$

with $$\varepsilon = \frac{\text{maximum velocity}}{\text{mean velocity}} - 1.0 \quad (2.7a)$$

or $$\varepsilon = \frac{U_s}{U_j} - 1.0 \quad (2.7b)$$

and also K_j was defined as

$$K_j = \frac{U_j}{U} \quad (2.8)$$

For the separation pressure coefficient C_{P_s} , they recommended an empirical relation that was fitted curve from various approaches as shown in figure 2.6.

And then progressed to compare the result of developed formula (the curve line)with many previous workers in figure 2.7.

From figure 2.7 , a reasonably good agreement is found between the experimental values and equation (2.5).

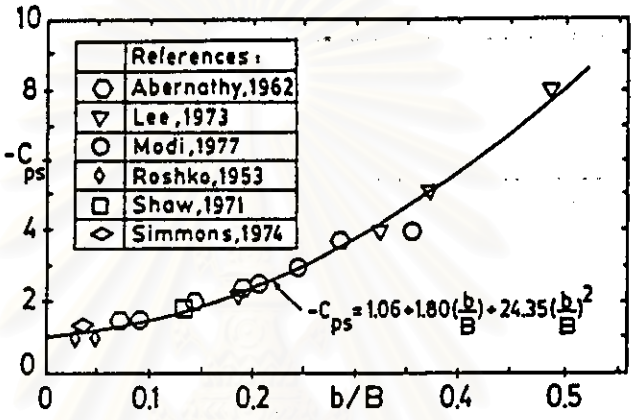

Figure 2.6 Variation of ($-C_{P_s}$) with b / B.

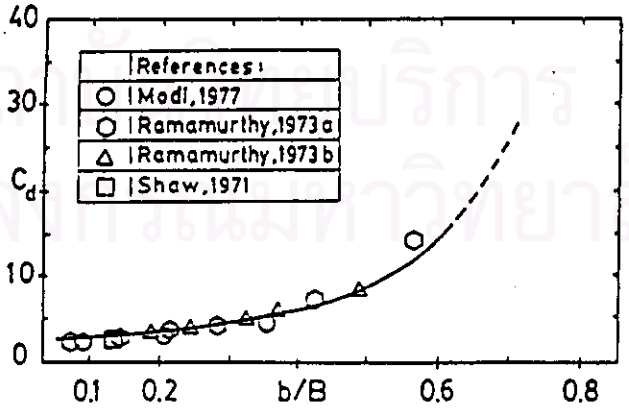

Figure 2.7 Variation of C_D with b / B ($0.20 \leq Re \times 10^{-5} \leq 3.0$).

2.2 FLOW SEPARATION OF INTERNAL FLOWS

The phenomenon of flow separation of internal flows caused by abrupt and sudden changes in the flow area has been studied extensively because of its technical importance.

Cherdron , Durst and Whitelaw (1978) observed experiments on asymmetric separation of internal laminar flows (or low Reynolds number sudden-expansion flows). This asymmetry occurs in spite of symmetric inlet profiles and the symmetry of the test-section geometry. The results suggest that the origin of the asymmetry is related to the shear layers and to coherent flow structures embedded in the random velocity fluctuation. Such structures exist in shear layers and can interact with each other , yielding phenomena that dominate the flow characteristics.

Figure 2.8 presents , in isometric projection , the development of the velocity profiles for two Reynolds numbers that correspond to the range in which asymmetric flow patterns were observed by flow-visualization techniques : the asymmetry about the x , z plane at y = 0 is confirmed by the measured velocity profiles. With boundary conditions of this type , a symmetric flow is usually expected and presumed in flow predictions , where half a test-section is considered for the solution domain. Calculations performed with presumed symmetric boundary conditions would lead to erroneous results for the present flows.

Figure 2.9 presents the velocity profiles at z = 0 and allows the recirculation to be identified more readily. It also shows that the lowerReynolds number flow has returned to a symmetric velocity distribution at avalue of x / H

of 16. The higher Reynolds number flow , on the other hand , still has a very asymmetric velocity distribution at x / H = 16 and has almost maintained the initial maximum velocity over the range of measurements.

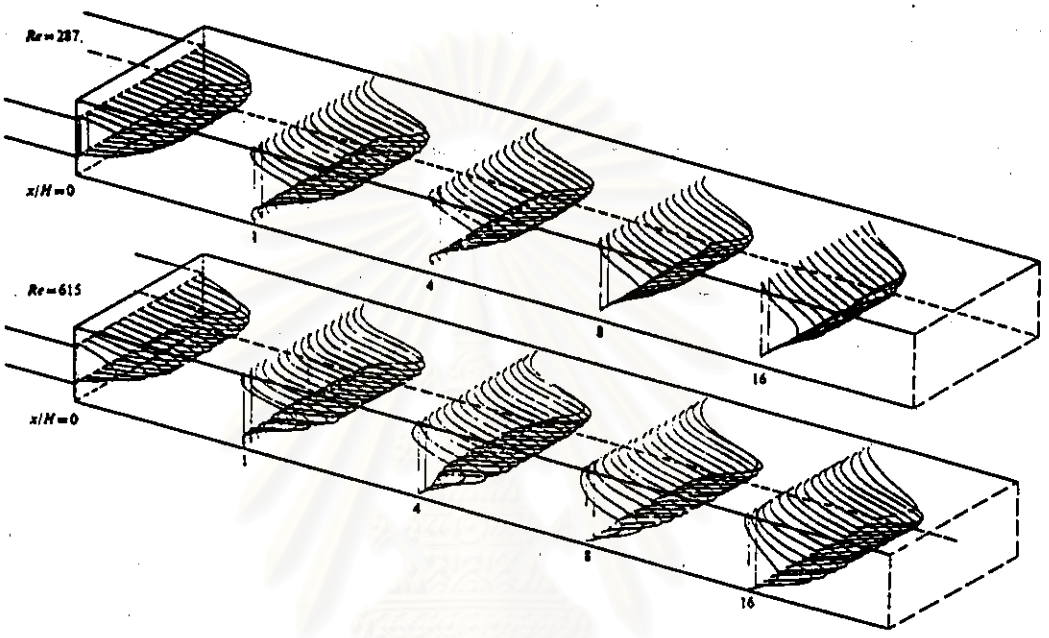

Figure 2.8 Mean velocity profiles.

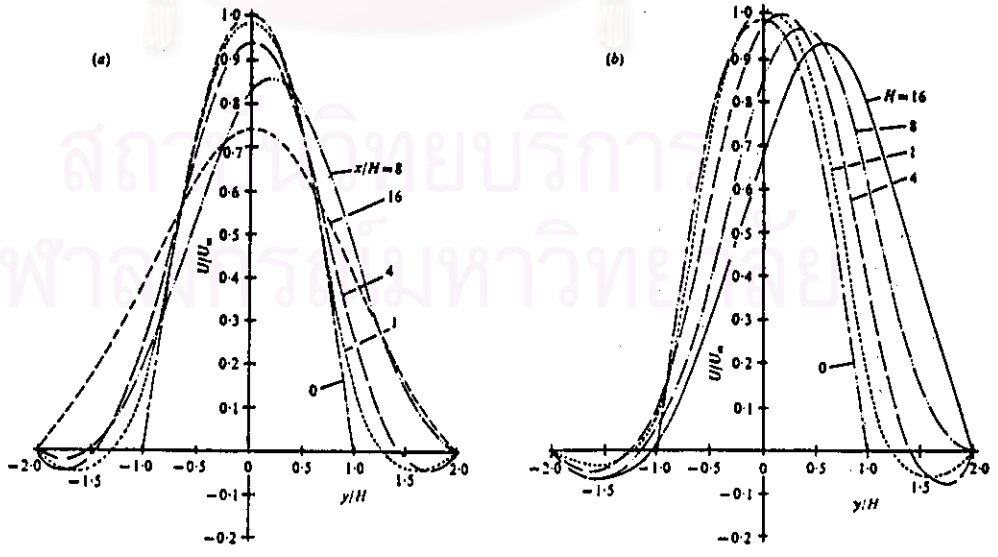

Figure 2.9 Velocity profiles in the symmetry (x , y) plane for an aspect ratio of 2 , an expansion ratio of 2 and a Reynolds number of (a) 287 and (b) 615.

Durst and Rastogi (1979) invested the flow visualization experiments of turbulent flows with separation and also used the finite difference solution procedures for calculating in the redevelopment region by the computer program *GENMIX*. The two-dimensional form of the continuity and the time-averaged Navier-Stokes equations were carried out to solve with both k-ε and the three-equation k-ε-$\overline{u'v'}$ turbulence model. The calculations are compared with the measurements and demonstrate clearly that use of the three-equation model improves the calculated profiles further but not significantly and not offer worthwhile advantages over the two-equation k-ε turbulence model as shown in figure 2.10.

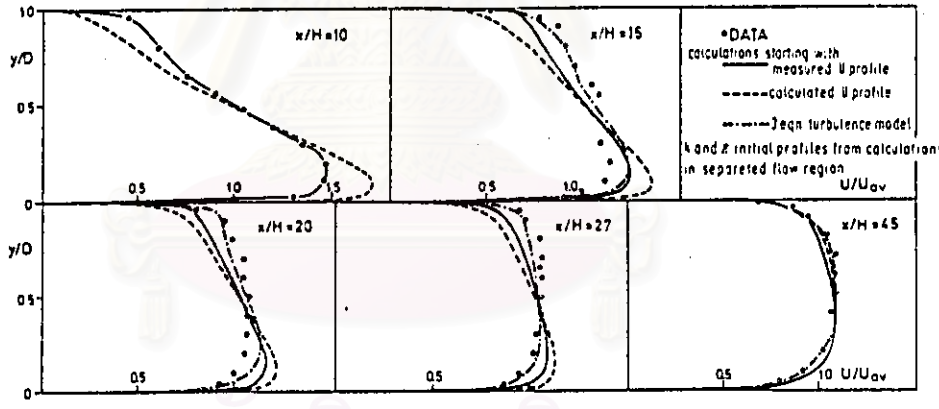

Figure 2.10 Measured and calculated U or $\overline{u}$ profiles in the boundary-layer region.

Armaly , Durst , Pereira and Schönung (1983) invested the experiment of laminar , transitional and turbulent flows with regions of separation behind a two-dimensional backward-facing step were carried out , and confirmed that

laser-doppler measurements can provide detailed information on the flow structure in the entire flow regime. The length of the recirculating-flow region in the immediate vicinity of the backward-facing step was measured and its strong dependence on Reynolds number was quantified as shown in figure 2.11. In the laminar-flow regime the separation length increased with increasing Reynolds number. A further increase in Reynolds number caused the velocity fluctuations to increase , indicating the beginning of transition to turbulent flow. It is shown that transition from laminar to turbulent flow is characterized by an initially strong decrease in the main separation region attached to the step. Moreover , a recirculating-flow region was also observed on the test-section wall opposite to the step which initially increased and thendecreased in size with increasing Reynolds number and decayed when the flow became fully turbulent.

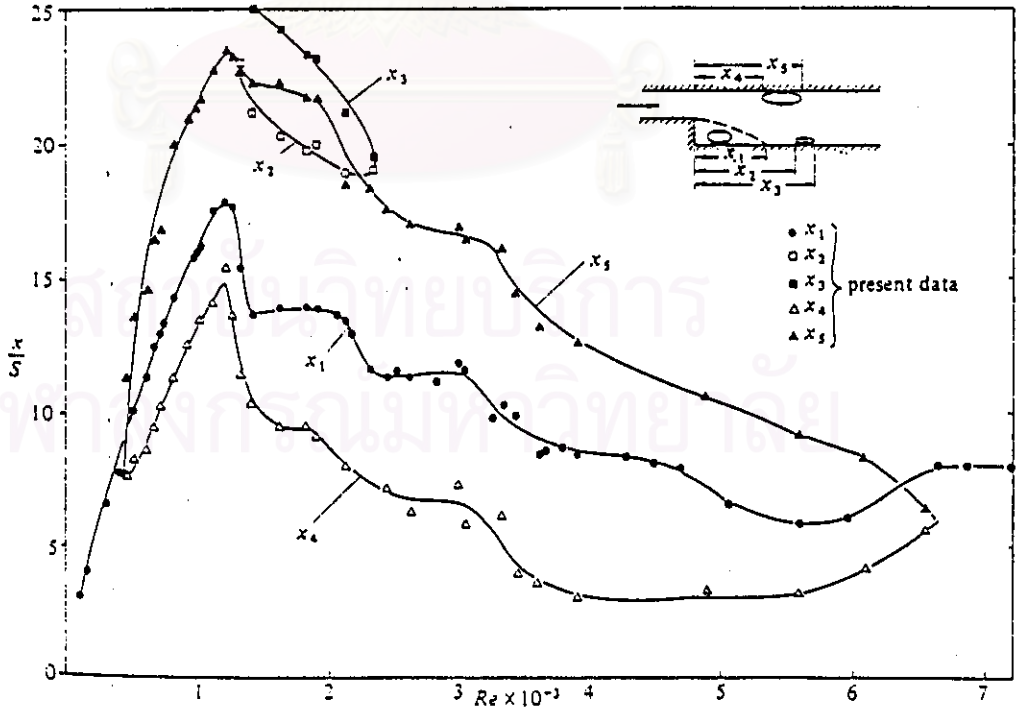

Figure 2.11 Location of detachment and reattachment of the flow at the centre of the test-section ; variation of locations with Reynolds number.
(where S is the step height)

Nallasamy (1986) studied on the steady separated flow due to an obstruction in a two-dimensional channel by the numerical solution of the Navier-Stokes equations from finite difference techniques. The effect of the inlet velocity profile on the separated region behind the obstruction was investigated at a Reynolds number of 100. A notable feature is that the separated regions have the same length for both uniform and parabolic inlet velocity profiles. This is due to the accelerating nature of the flow at the section of the constriction resulting in nearly the same velocity profiles there for the two cases (see figure 2.12). That is , due to the constriction , the separating layers have the same strength. This is in contrast to the flow over abackward-facing step where the separated region behind the step is a distinctfunction of the inlet velocity profile.

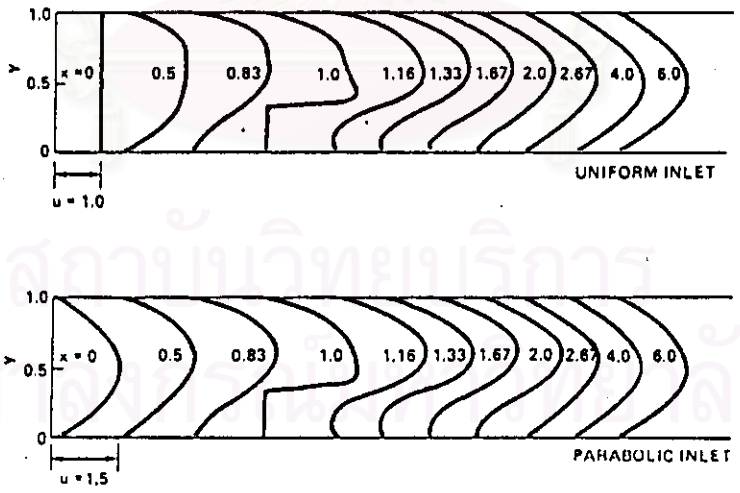

Figure 2.12 Effect of inlet velocity profile.